Compressive Hyperspectral Imaging using Coded Fourier Transform Interferometry

Amirafshar Moshtaghpour*, Valerio Cambareri*, Laurent Jacques*, Philippe Antoine† and Matthieu Roblin†
*ICTEAM, Université catholique de Louvain, Belgium (funded by Belgian F.R.S.-FNRS). †Lambda-X SA, Nivelles, Belgium

***Abstract*—Fourier Transform Interferometry (FTI) is a Hyperspectral (HS) imaging technique that is specially desirable in high spectral resolution applications, such as spectral microscopy in biology. The current resolution limit of FTI is actually due to the durability of biological elements when exposed to illuminating light. We propose two variants of the FTI imager, *i.e.*, coded illumination-FTI and coded aperture-FTI, that efficiently allocate the illumination distribution with a *variable density sampling* strategy, so that the exposure time of the biological specimen is minimized while spectral resolution is preserved. We derive a theoretical analysis for both proposed methods. Our results are supported by several experimental simulations.**

I. Introduction

Among a plethora of different hyperspectral (HS) image acquisition techniques, Fourier Transform Interferometry (FTI) has received a renewed interest for its high spectral resolution capability; a key criterion for, *e.g.*, biomedical fluorescence spectroscopy [1]. FTI consists in a Michelson interferometer where one mirror of its two arms is moved to modify the Optical Path Difference $\xi \in \mathbb{R}$ (OPD) of the system (see Fig. 1 for details). For each OPD ξ and each pixel location $(x, y) \in \mathbb{R}^2$ of an imaging sensor, an interferometric signal is then recorded in a volume $\mathcal{Y}(\xi; x, y)$. Physical optics then shows that $\mathcal{Y}$ is the Fourier transform, with respect to wavenumber ν, of the HS image $\mathcal{X}(\nu; x, y)$ [2], *i.e.*, ξ and ν are dual parameters. From the Shannon-Nyquist theorem, for a fixed OPD sampling period Δ_ξ and interval $N_\xi \Delta_\xi$ (with N_ξ samples), an HS image with wavenumber resolution $2\pi/(N_\xi \Delta_\xi)$ and range π/Δ_ξ can be reached.

In FTI, the total illumination imposed on the biological specimen is proportional to N_ξ for a constant light source. Since over-exposed biological elements suffer photochemical changes, *i.e.*, *photo-bleaching* [1], the number of FTI measurements needs to be minimized while keeping good HS image quality.

In this paper, we propose two schemes ensuring that the desired resolution is preserved while the exposure time (and with it photo-bleaching) is significantly reduced. Both schemes amount to an incomplete set of FTI measurements. Recovering a high resolution HS image from such under-sampled data is demanding: conventional methods, *e.g.*, minimum energy solution, produce poor quality images, while we show how the framework of compressive sensing [3, 4] and the notion of *variable density sampling* (VDS) [5] yields conspicuous quality improvements.

II. Proposed Methods

We study FTI in a simplified setting where the HS image is a matrix $\boldsymbol{X} \in \mathbb{R}^{N_\xi \times N_p}$ approximating $\mathcal{X}$ over N_p pixels and N_ξ OPD samples. In this context, we analyze two different sensing scenarios in which a measurement vector $\boldsymbol{y} \in \mathbb{C}^M$ is observed by:

$$\boldsymbol{y} = \boldsymbol{\Phi}_\Omega \boldsymbol{x} + \boldsymbol{n}, \qquad \boldsymbol{\Phi}_\Omega := \boldsymbol{R}_\Omega \boldsymbol{\Phi} = \boldsymbol{R}_\Omega (\boldsymbol{I}_{N_p} \otimes \boldsymbol{F}_{N_\xi}), \quad (1)$$

where $\boldsymbol{x} \in \mathbb{R}^N$ is the vectorization of $\boldsymbol{X}$ (with $N = N_\xi N_p$), $\boldsymbol{R}_\Omega \in \{0,1\}^{M \times N}$ is the operator extracting the $M = |\Omega|$ rows of a matrix indexed in $\Omega \subset [N] := \{1, \cdots, N\}$, $\boldsymbol{F}_{N_\xi} \in \mathbb{C}^{N_\xi \times N_\xi}$ is the DFT matrix, $\boldsymbol{I}_{N_p} \in \mathbb{R}^{N_p \times N_p}$ is the identity matrix, $\boldsymbol{n} \in \mathbb{R}^M$ is an additive measurement noise, and $\otimes$ is the Kronecker product.

(i) Coded Illumination-FTI (CI-FTI): In CI-FTI we activate the light source during $M_\xi \ll N_\xi$ time slots[1], as shown in Fig. 2 (top). In this case $\boldsymbol{y}$ is denoted by $\boldsymbol{y}^{\text{CI}}$ and Ω is separable in the following sense: $\boldsymbol{R}_\Omega(\boldsymbol{I}_{N_p} \otimes \boldsymbol{F}_{N_\xi}) = \boldsymbol{I}_{N_p} \otimes \boldsymbol{R}_{\Omega^\xi} \boldsymbol{F}_{N_\xi}$ with $\Omega^\xi \subset [N_\xi]$ that corresponds to the indices of active OPDs (*i.e.,* time slots).

(ii) Coded Aperture-FTI (CA-FTI): In this approach, the illumination is *coded* so that, at each OPD sample only a group of spatial locations of the specimen are exposed. This can be done by using a coded aperture pattern or a spatial light modulator [7, 8], as shown in Fig. 2 (bottom). In this case, $\boldsymbol{y} = \boldsymbol{y}^{\text{CA}}$ and Ω is no more separable.

III. Main Results

Our main results leverage [5] for both sensing schemes in order to determine an optimal VDS of $[N]$, *i.e.*, an optimal *probability mass function* (pmf) $p(i) := \mathbb{P}[S = i]$ of a random variable (r.v.) $S \in [N]$ such that $\Omega = \{\Omega_1, \cdots, \Omega_M\} \subset [N]$ with $\Omega_i \sim_{\text{iid}} S$. A stable and robust HS recovery is then reached by solving

$$\hat{\boldsymbol{x}} = \arg\min_{\boldsymbol{u} \in \mathbb{R}^N} \|\boldsymbol{\Psi}^T \boldsymbol{u}\|_1 \text{ s.t. } \|\boldsymbol{D}(\boldsymbol{y} - \boldsymbol{\Phi}_\Omega \boldsymbol{u})\|_2 \leq \varepsilon \sqrt{M}, \quad (2)$$

where $\boldsymbol{\Psi} \in \mathbb{R}^{N \times N}$ is an (analysis) sparsity basis and $\boldsymbol{D} \in \mathbb{R}^{M \times M}$ is a diagonal matrix such that $D_{ii} = 1/p(\Omega_i)^{1/2}$ [5]. Notice that in CI-FTI, from the separability of Ω, $\boldsymbol{D} := \boldsymbol{I}_{N_p} \otimes \boldsymbol{D}_\xi$ where $(\boldsymbol{D}_\xi)_{jj} = 1/p_\xi(\Omega^\xi_j)^{1/2}$ for some pmf p_ξ over $[N_\xi]$.

The importance of this VDS scheme introduced in [5] is twofold. First, VDS lifts the sample complexity barrier met by uniform density sampling (UDS) where p is constant. Second, the resulting matrix $M^{-\frac{1}{2}} \boldsymbol{D} \boldsymbol{\Phi}_\Omega \boldsymbol{\Psi}$ satisfies with high probability the *restricted isometry property* resulting in uniform signal recovery guarantee [5, 9]. In fact, given some $\theta = \theta(\boldsymbol{\Phi}, \boldsymbol{\Psi}) > 0$, for UDS and VDS, we must have $M = O(\theta^2 K \log^3(K) \log(N))$ in order to reconstruct K-sparse signals via (2). For UDS, $\theta := \sqrt{N} \max_{ij} |(\boldsymbol{\Phi}\boldsymbol{\Psi})_{ij}|$ is the *mutual coherence* between $\boldsymbol{\Phi}$ and $\boldsymbol{\Psi}$, with $\theta \approx \sqrt{N}$ and $M \approx N$ for the Fourier-Haar system. The VDS proposed in [5] links Ω to the non-constant pmf $p(i) = \kappa_i^2 / \|\boldsymbol{\kappa}\|_2^2$ with the *local coherence* $\kappa_i := \max_j |\boldsymbol{\Phi}\boldsymbol{\Psi}|_{ij}$, and $\theta = \|\boldsymbol{\kappa}\|_2$. Computation of $\boldsymbol{\kappa}$ for the Fourier-Haar system gives $M = O(K \log^3(K) \log^2(N))$ and $p(i)$ inversely proportional to the OPD magnitude.

In (2), in accordance with CA/CI-FTI adjusted to this pmf, we thus follow a VDS scheme and decide to promote a 3D sparsity model with respect to $\boldsymbol{\Psi} := \boldsymbol{\Psi}_{\text{2D}} \otimes \boldsymbol{\Psi}_{\text{1D}}$, where $\boldsymbol{\Psi}_{\text{2D}}$ and $\boldsymbol{\Psi}_{\text{1D}}$ are the 2D and 1D Haar wavelet bases with respect to the spatial and the spectral domain, respectively. This allows for an efficient representation of both the spatial and spectral variations of a biological sample mixed several fluorochromes (Fig. 3).

Correspondingly, using a VDS-driven FTI, we show first that in CI-FTI HS images are recovered from $M_\xi = O(\bar{K} \log^3(\bar{K}) \log(N))$ time slots, *i.e.*, $N_p M_\xi$ measurements, where $\bar{K} = \max_i \|(\boldsymbol{\Psi}_{\text{1D}} \boldsymbol{X} \boldsymbol{\Psi}_{\text{2D}}^T)_{:,i}\|_0 \leq N_\xi$ is the worst column (or spectral) sparsity of the HS image. Second, for CA-FTI, we need $M = O(K \log^3(K) \log^2(N))$ measurements with K the total sparsity of the HS image in $\boldsymbol{\Psi}$.

Therefore, while the two sensing schemes allow for compressive FTI, we can expect that $K \leq N_p \bar{K}$ for biological samples where the pixels that display complex spectral signatures are supported by a minority of spatial wavelet coefficients. Therefore CA-FTI should then require a smaller number of measurements, and thus a smaller light exposure, than CI-FTI for successful HS image reconstructions, as confirmed in the synthetic example of Fig. 4. The realization of an actual CI/CA-FTI device (with possible sensing discrepancies *e.g.,* Poisson noise) is ongoing.

[1] This accords with subsampling mirror positions in [6].

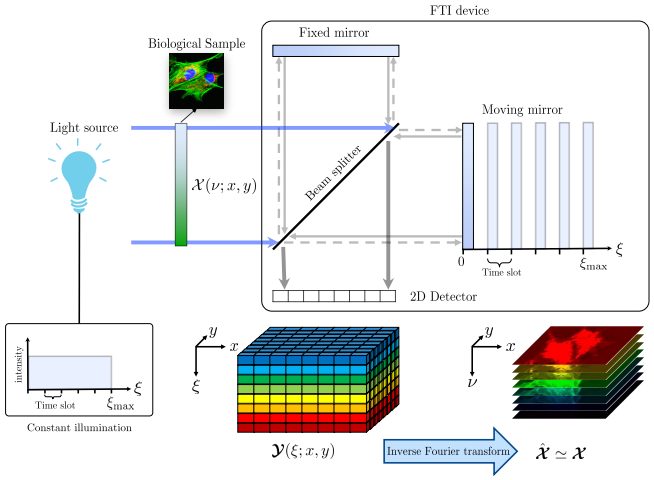

Fig. 1: FTI operating principles. The HS input denoted by $\mathcal{X}$ corresponds here to the optical HS output of a fluorescence microscope, *i.e.*, the magnified hyperspectral image of the sample. The light beam coming from the sample is divided into equal intensity beam by the splitter. The two beams are reflected back by the respective mirrors. Besides, the phase shift between two beams, termed as Optical Path Difference (OPD) ξ, changes with respect to the position of the moving mirror. The two beams interfere after being recombined by the beam-splitter. The resulting beam is later recorded (in intensity) by an imaging sensor, which captures one image with N_p pixels per ξ, hence sampling $\mathcal{Y}$. In classical FTI, an inverse Fourier transform applied on this recording gives an estimate $\hat{\mathcal{X}} \approx \mathcal{X}$. For simplicity of the schematic, all imaging optics are also omitted.

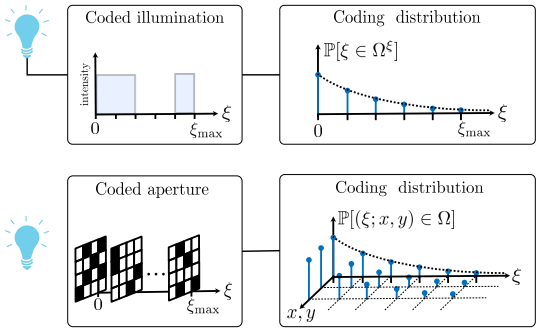

Fig. 2: Illustration of (top) CI-FTI and (bottom) CA-FTI with, for both cases, the corresponding probability mass function p adjusting the VDS.

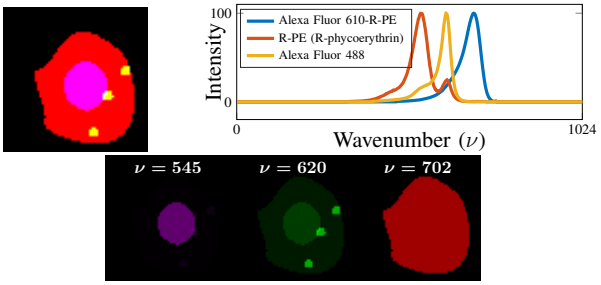

Fig. 3: A synthetic ground truth HS volume is generated by mixing an RGB image (top left), *i.e.*, taken from [10], with the known spectral signatures of three actual fluorescent dyes (top right). (Bottom) Three spatial maps.

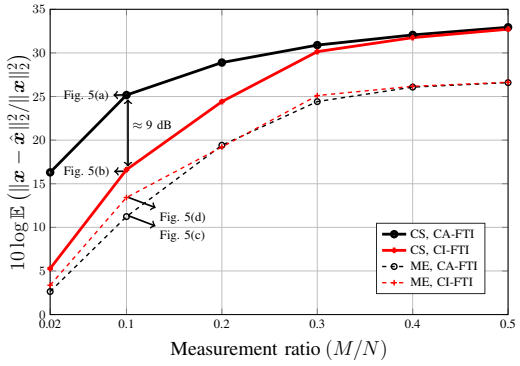

Fig. 4: Reconstruction performance of Minimum Energy (ME) (*i.e.*, applying the pseudo-inverse of $\boldsymbol{\Phi}_\Omega$) and Compressive Sensing (CS) frameworks for CA-FTI and CI-FTI. The results are averaged over 10 trials (*i.e.*, over the random selection of Ω). Noise level is set such that $10\log\left(\|\boldsymbol{D}\boldsymbol{\Phi}_\Omega\boldsymbol{x}\|_2^2/\|\boldsymbol{D}\boldsymbol{n}\|_2^2\right) = 10$ dB. As explained in the text (and also by the $\ell_2-\ell_1$ instance optimality of (2) [5]) CA-FTI needs less number of samples than CI-FTI. Moreover, regardless of measurement ratio ME solution results in poor quality images.

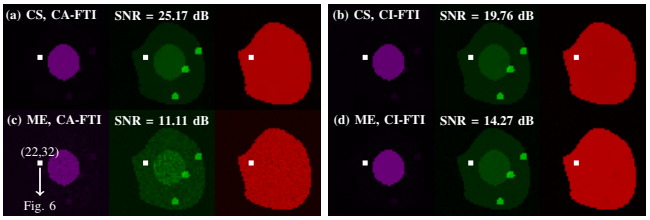

Fig. 5: An example of the reconstructed HS image from 10% of the total measurements (illumination). The quality of the reconstruction is obvious both visually, with respect to Fig. 3(bottom), and quantitatively; although, our objective is to provide high spectral resolution HS images. The ability of proposed methods in preserving the spectral resolution is shown in Fig. 6, for the point indicated by a white square.

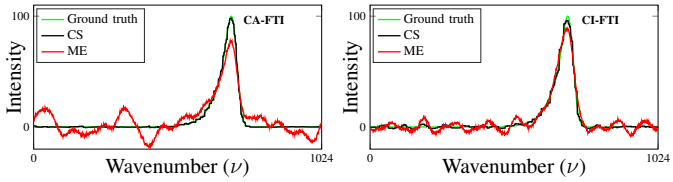

Fig. 6: The spectrum of the reconstructed HS image in Fig. 5 at pixel location $(22, 32)$. The sidebands in the ME reconstruction considerably degrades the accuracy of the HS acquisition; while in CS reconstruction the shape of the spectrum is well-preserved.

References

[1] G. Lu and B. Fei, "Medical hyperspectral imaging: a review," *Journal of biomedical optics*, vol. 19, no. 1, pp. 010 901–010 901, 2014.

[2] R. Bell, *Introductory Fourier transform spectroscopy*. Elsevier, 2012.

[3] D. L. Donoho, "Compressed sensing," *IEEE Transactions on information theory*, vol. 52, no. 4, pp. 1289–1306, 2006.

[4] E. J. Candes and T. Tao, "Near-optimal signal recovery from random projections: Universal encoding strategies?" *IEEE transactions on information theory*, vol. 52, no. 12, pp. 5406–5425, 2006.

[5] F. Krahmer and R. Ward, "Stable and robust sampling strategies for compressive imaging," *IEEE transactions on image processing*, vol. 23, no. 2, pp. 612–622, 2014.

[6] A. Moshtaghpour, K. Degraux, V. Cambareri, A. Gonzalez, M. Roblin, L. Jacques, and P. Antoine, "Compressive hyperspectral imaging with fourier transform interferometry," in *3rd international International Traveling Workshop on Interactions between Sparse models and Technology*, 2016, pp. 27–29.

[7] M. Gehm, R. John, D. Brady, R. Willett, and T. Schulz, "Single-shot compressive spectral imaging with a dual-disperser architecture," *Optics express*, vol. 15, no. 21, pp. 14 013–14 027, 2007.

[8] M. F. Duarte, M. A. Davenport, D. Takhar, J. N. Laska, T. Sun, K. E. Kelly, R. G. Baraniuk *et al.*, "Single-pixel imaging via compressive sampling," *IEEE Signal Processing Magazine*, vol. 25, no. 2, p. 83, 2008.

[9] E. J. Candes and T. Tao, "Decoding by linear programming," *IEEE transactions on information theory*, vol. 51, no. 12, pp. 4203–4215, 2005.

[10] P. Ruusuvuori, A. Lehmussola, J. Selinummi, T. Rajala, H. Huttunen, and O. Yli-Harja, "Benchmark set of synthetic images for validating cell image analysis algorithms," in *16th European Signal Processing Conference*, 2008, pp. 1–5.